Supplementary Information for
Biophysical comparison of ATP synthesis mechanisms shows a kinetic advantage for the rotary process

Ramu Anandakrishnan, Zining Zhang, Rory Donovan and Daniel M. Zuckerman

---

In the main text we analyzed the kinetics of the rotary and other possible mechanisms coupling proton transport to ATP synthesis, using the kinetic cycles shown in Fig. S1. Additional supporting information for that analysis is presented here: (1) the full set of kinetic diagrams, (2) derivation of the thermodynamic cycle constraint, (3) derivation of the non-equilibrium steady state solution for a single cycle kinetic system, (4) the range of conditions used in the analysis, (5) the range of parameter values used in the analysis, (6) details of the sensitivity analysis, and (7) a test of 4:1 H^+:ATP stoichiometry.

1. Full set of kinetic diagrams

The ATP synthesis cycle can be represented by a sequence of ten reactions (events) as depicted in Fig. S1. The rate constants (k) for each reaction, shown in the figure, are described in the *Range of parameter values* section below . A key differentiating characteristic of the rotary mechanism compared to the basic alternating access mechanism, for ATP synthesis, is the order of proton binding and transport. In the rotary mechanism protons bind to the membrane-spanning F_o subunit of the ATP synthase facing the lower pH/higher proton concentration side ("in"-side) of the membrane, and are transported across the membrane (to the "out"-side) one-at-a-time [1]. In contrast, in the basic alternating access mechanism multiple protons bind to the low pH side of the ATPase and are transported across the membrane simultaneously [2]. For the analysis presented here we compared all five possible proton transport orderings for a 3:1 H^+:ATP stoichiometry, as shown in Fig. S1. Note that additional non-ion event orders (e.g., ADP, Pi binding) are considered in SI section 6 on sensitivity analysis.

2. Thermodynamic cycle constraint

All of the kinetic cycles represented in Fig. S1 place a thermodynamic constraint on the kinetic parameters due to the requirement that the free energy change for the ATP synthesis cycle, which is the driving potential $\Delta G_{\rm driv}$, must be equal to the sum of the free energy changes for each of the steps in the cycle [3], i.e.

$$\Delta G_{\rm driv} = \sum_i^s G_i - G_{i+1} \tag{1}$$

where the basic free energy (FE) G_i for state i is defined in terms of the effective first order rate constants $\alpha_{i,j}$ by

$$G_{i-1} - G_i = -(1/\beta)\ln(\alpha_{i,i-1}/\alpha_{i-1,i}) \tag{2}$$

where $\alpha_{i,j} = c_i k_{i,j}$ is the effective first order rate constant, with $c = 1$ for a first order process and $c = [X]$ when species X binds in the transition from state i to j, and $k_{i,j}$ is the corresponding rate constant; $\beta = 1/k_B T$ where k_B is the Boltzmann constant and T is the temperature. $\Delta G_{\rm driv}$ is also defined as

$$\Delta G_{\rm driv} = n(-F\Delta\psi + 2.3RT\Delta{\rm pH}) - \Delta G_{\rm ATP} \tag{3}$$

$$\Delta G_{\rm ATP} = \Delta G^0 + RT\ln([ATP]/[ADP][Pi]) \tag{4}$$

$$10^{\Delta{\rm pH}} = [H^+_{\rm out}]/[H^+_{\rm in}] \tag{5}$$

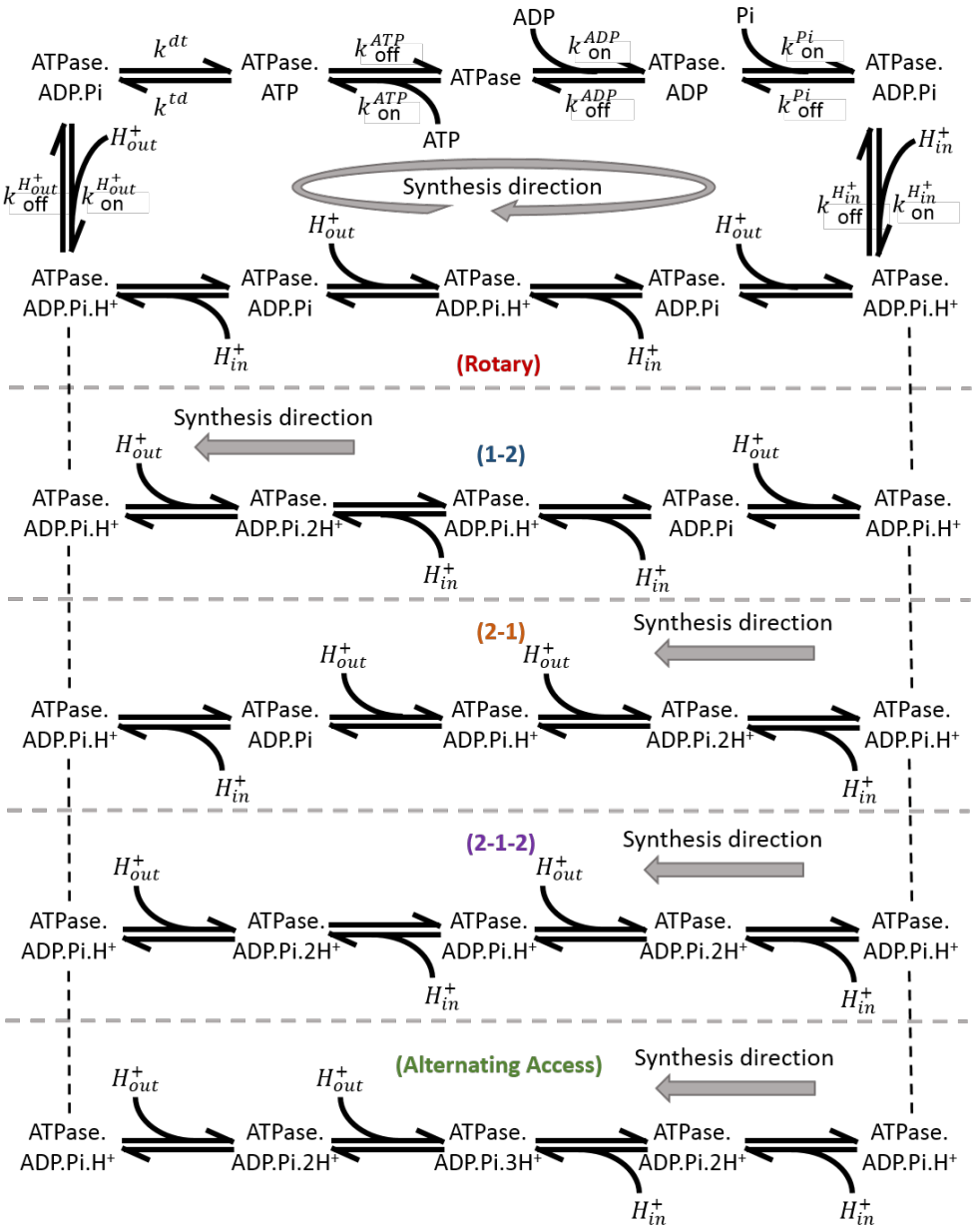

Figure S1: Minimalist kinetic modeling of rotary and alternative mechanisms for ATP synthesis. Synthesis cycles for the rotary, basic alternating access and other possible mechanisms based on proton transport order for a 3:1 H^+:ATP stoichiometry. Note that conformational processes, such as rotation are implicitly included in the binding and chemical processes shown in a thermodynamically consistent way.

where $\Delta\psi = \psi_{\rm out} - \psi_{\rm in}$ is the trans-membrane potential and $\Delta{\rm pH} = {\rm pH}_{\rm out} - {\rm pH}_{\rm in}$ is the pH difference (the "out"-side is the higher pH catalytic side of the membrane and the "in"-side is the lower pH side of the membrane [4]); $\Delta G_{\rm ATP}$ is the free energy required for ATP synthesis for the given concentrations of ADP, ATP and Pi under ideal-solution assumptions; ΔG^0 is the free energy required for ATP synthesis under the conditions considered. Since ΔG^0 depends on pH [5], we use different values for ΔG^0 depending on pH. See Sensitivity Analysis below. F is the Faraday constant and R is the gas constant. The ratio $\alpha_{i,i+1}/\alpha_{i+1,i} = c_i k_{i,i+1}/c_{i+1}k_{i+1,i} = c_i K/c_{i+1}$ where K is the step-specific equilibrium constant. From Eqs. (1)–(5), along with this relationship between the ratio of effective first order rate constants $\alpha_{i,j}$ and the

equilibrium constant K, we have

$$e^{3\beta F\Delta\psi} = \frac{K_d^{ATP}}{K_d^{ADP}K_d^{Pi}K^{dt}} \left(\frac{K_d^{H^+_{\text{in}}}}{K_d^{H^+_{\text{out}}}}\right)^3 e^{-\beta\Delta G^0} \tag{6}$$

The above relationship is similar to one previously suggested by [6]. The same constraint holds for all five mechanisms considered. Note that only the equilibrium constants and the two driving components of proton motive force enter the constraint. To enforce this thermodynamic constraint in our model, we chose to vary the rate constant $k_{\text{off}}^{H^+_{\text{out}}}$ with $\Delta\psi$, while using the optimization protocol described in the main text for setting all other rate constants, i.e. from Eq. (6),

$$k_{\text{off}}^{H^+_{\text{in}}} = \left(K_d^{ADP}K_d^{Pi}K^{dt}/K_d^{ATP}\right)^{1/3} K_d^{H^+_{\text{out}}} k_{\text{on}}^{H^+_{\text{in}}} e^{\beta\Delta G^0} e^{\beta F\Delta\psi} \tag{7}$$

However, the parameter value calculated from the thermodynamic constraint also varies in the optimization process, described in the main text. Therefore, the resulting set of optimized parameter values do not depend on which specific parameter is constrained.

3. Non-equilibrium steady state solution for a single cycle kinetic system

Presented here is an alternative to a previous derivation [7] of a closed-form steady-state solution for a single cycle chemical process. The final formulation presented below (Eq. (23)) is stated in terms of free energies instead of rate constants, which can provide physical insight into the relationship between the thermodynamics and kinetics of the system. For a single-cycle kinetic model, such as the one shown in Fig. S1, by definition the steady state rate can be calculated as the flow J between any two states

$$J = p_i\alpha_{i,i+1} - p_{i+1}\alpha_{i+1,i} \tag{8}$$

where p_i is the steady-state probability of state i. For a single cycle kinetic system with s states:

$$\begin{aligned}
J &= p_1\alpha_{1,2} - p_2\alpha_{2,1} && (9)\\
J &= p_2\alpha_{2,3} - p_3\alpha_{3,2} && (10)\\
&\vdots \\
J &= p_{s-1}\alpha_{s-1,s} - p_s\alpha_{s,s-1} && (11)\\
J &= p_s\alpha_{s,1} - p_1\alpha_{1,s} && (12)
\end{aligned}$$

By substitution, each of the probabilities p_i can be expressed in terms of J and p_1. Using the definition $r_i = \alpha_{i+1,i}/\alpha_{i,i+1}$,

$$
\begin{aligned}
p_s &= p_1 r_1 + \frac{J}{\alpha_{s,1}} && (13)\\
p_{s-1} &= p_s r_s + \frac{J}{\alpha_{s-1,s}} \\
&= \left(p_1 r_1 + \frac{J}{\alpha_{s,1}}\right) r_s + \frac{J}{\alpha_{s-1,s}} \\
&= p_1 r_1 r_s + \frac{J}{\alpha_{s,1}} r_s + \frac{J}{\alpha_{s-1,s}} && (14)\\
p_{s-2} &= p_{s-1} r_{s-1} + \frac{J}{\alpha_{s-2,s-1}} \\
&= \left(p_1 r_1 r_s + \frac{J}{\alpha_{s,1}} r_s + \frac{J}{\alpha_{s-1,s}}\right) r_{s-1} + \frac{J}{\alpha_{s-2,s-1}} \\
&= p_1 r_1 r_s r_{s-1} + \frac{J}{\alpha_{s,1}} r_s r_{s-1} + \frac{J}{\alpha_{s-1,s}} r_{s-1} + \frac{J}{\alpha_{s-2,s-1}} && (15)\\
&\vdots \\
p_2 &= p_3 r_3 + \frac{J}{\alpha_{2,3}} \\
&= \left(\left(\cdots\left(\left(p1 r_1 + \frac{J}{\alpha_{s,1}}\right) r_s + \frac{J}{\alpha_{s-1,s}}\right) r_{s-1} + \cdots\right) r_4 + \frac{J}{\alpha_{3,4}}\right) r_3 + \frac{J}{\alpha_{2,3}} \\
&= p_1 (r_1 r_s \cdots r_4 r_3) + \frac{J}{\alpha_{s,1}} (r_s r_{s-1} \cdots r_4 r_3) + \frac{J}{\alpha_{s-1,s}} (r_{s-1} r_{s-2} \cdots r_4 r_3) + \cdots \\
&\quad + \frac{J}{\alpha_{4,5}} r_4 r_3 + \frac{J}{\alpha_{3,4}} r_3 + \frac{J}{\alpha_{2,3}} && (16)\\
p_1 &= p_2 r_2 + \frac{J}{\alpha_{1,2}} \\
&= \left(\left(\cdots\left(\left(p_1 r_1 + \frac{J}{\alpha_{s,1}}\right) r_s + \frac{J}{\alpha_{s-1,s}}\right) r_{s-1} + \cdots\right) r_3 + \frac{J}{\alpha_{2,3}}\right) r_2 + \frac{J}{\alpha_{1,2}} \\
&= p_1 (r_1 r_s \cdots r_3 r_2) + \frac{J}{\alpha_{s,1}} (r_s r_{s-1} \cdots r_3 r_2) + \frac{J}{\alpha_{s-1,s}} (r_{s-1} r_{s-2} \cdots r_3 r_2) + \cdots \\
&\quad + \frac{J}{\alpha_{3,4}} r_3 r_2 + \frac{J}{\alpha_{2,3}} r_2 + \frac{J}{\alpha_{1,2}} && (17)
\end{aligned}
$$

From Eq. (17), p_1 can be expressed in terms of J and the effective first order rate constants as

$$
p_1 = \frac{J}{1-X}\left[\frac{(r_s r_{s-1} \cdots r_3 r_2)}{\alpha_{s,1}} + \frac{(r_{s-1} r_{s-2} \cdots r_3 r_2)}{\alpha_{s-1,s}} + \cdots + \frac{r_3 r_2}{\alpha_{3,4}} + \frac{r_2}{\alpha_{2,3}} + \frac{1}{\alpha_{1,2}}\right] \qquad (18)
$$

where $X = r_1 r_2 \cdots r_s$. Substituting Eq. (18) into Eq. (13) – (16), and using the unity sum-rule for probability $\sum_i p_i = 1$, we find

$$
\begin{aligned}
\frac{1}{J} &= \frac{1}{1-X}\left[\frac{X}{\alpha_{s,1}} + \frac{r_{s-1}\cdots r_1}{\alpha_{s-1,s}} + \cdots + \frac{r_2 r_1}{\alpha_{2,3}} + \frac{r_1}{\alpha_{1,2}}\right] + \frac{1}{\alpha_{s,1}} \\
&\quad + \frac{1}{1-X}\left[\frac{X r_s}{\alpha_{s,1}} + \frac{X}{\alpha_{s-1,s}} + \cdots + \frac{r_2 r_1 r_s}{\alpha_{2,3}} + \frac{r_1 r_s}{\alpha_{1,2}}\right] + \frac{r_s}{\alpha_{s,1}} + \frac{1}{\alpha_{s-1,s}} \\
&\quad \vdots \\
&\quad + \frac{1}{1-X}\left[\frac{X(r_s r_{s-1}\cdots r_3)}{\alpha_{s,1}} + \frac{X(r_{s-1}\cdots r_3)}{\alpha_{s-1,s}} + \cdots + \frac{X}{\alpha_{2,3}} + \frac{r_1 r_s \cdots r_3}{\alpha_{1,2}}\right] \\
&\quad + \frac{(r_s r_{s-1}\cdots r_3)}{\alpha_{s,1}} + \frac{(r_{s-1}\cdots r_3)}{\alpha_{s-1,s}} + \cdots + \frac{r_4 r_3}{\alpha_{4,5}} + \frac{r_3}{\alpha_{3,4}} + \frac{1}{\alpha_{2,3}} \\
&\quad + \frac{1}{1-X}\left[\frac{(r_s r_{s-1}\cdots r_2)}{\alpha_{s,1}} + \frac{(r_{s-1}\cdots r_2)}{\alpha_{s-1,s}} + \cdots + \frac{r_3 r_2}{\alpha_{3,4}} + \frac{r_2}{\alpha_{2,3}} + \frac{1}{\alpha_{1,2}}\right] \qquad (19) \\
&= \frac{1}{\alpha_{1,2}}\left[\frac{1 + r_1 + r_1 r_s + \cdots + (r_1 r_s \cdots r_3)}{1-X}\right] \\
&\quad + \frac{1}{\alpha_{2,3}}\left[\frac{r_2 + r_2 r_1 + r_2 r_1 r_s + \cdots + (r_2 r_1 \cdots r_4)}{1-X} + \frac{X}{1-X} + 1\right] \\
&\quad + \frac{1}{\alpha_{3,4}}\left[\frac{r_3 r_4 + r_3 r_4 r_5 + r_3 r_4 r_5 r_6 + \cdots + (r_3 r_4 \cdots r_1)}{1-X} + \frac{X(1+r_3)}{1-X} + (1+r_3)\right] \\
&\quad \vdots \\
&\quad + \frac{1}{\alpha_{s-1,s}}\left[\frac{(r_{s-1}\cdots r_2) + (r_{s-1}\cdots r_1)}{1-X} + \frac{X(1 + \cdots + (r_{s-1}\cdots r_3))}{1-X} + (1 + \cdots + (r_{s-1}\cdots r_3))\right] \\
&\quad + \frac{1}{\alpha_{s,1}}\left[\frac{r_s \cdots r_2}{1-X} + \frac{X(1 + r_s + \cdots + (r_s r_{s-1}\cdots r_3))}{1-X} + (1 + r_s + \cdots + (r_s r_{s-1}\cdots r_3))\right] \qquad (20) \\
&= \frac{1 + r_1 + r_1 r_s + \cdots + (r_1 r_s \cdots r_3)}{\alpha_{1,2}(1-X)} \\
&\quad + \frac{1 + r_2 + r_2 r_1 + \cdots + (r_2 r_1 \cdots r_4)}{\alpha_{2,3}(1-X)} \\
&\quad \vdots \\
&\quad + \frac{1 + r_{s-1} + r_{s-1} r_{s-2} + \cdots + (r_{s-1} r_{s-2} \cdots r_1)}{\alpha_{s-1,s}(1-X)} \\
&\quad + \frac{1 + r_s + r_s r_{s-1} + \cdots + (r_s r_{s-1} \cdots r_2)}{\alpha_{s,1}(1-X)} \qquad (21) \\
&= \frac{1}{1-X}\sum_{i=1}^{s} \frac{1}{\alpha_{i,i+1}}\left(1 + \sum_{j=0}^{s-2}\prod_{k=0}^{j} r_{i-j+k}\right) \qquad (22)
\end{aligned}
$$

For r_m in Eq. (22), if $m < 1$ then $m = s - m$ representing the corresponding state from the previous iteration of the cycle. For $\alpha_{i,i+1}$, if $i + 1 > s$ then $i + 1 = i + 1 - s$ representing the corresponding state from the following iteration of the cycle.

The basic free energy (FE) G_i for state i is defined in terms of the effective first order rate constants by $G_{i-1} - G_i = -(1/\beta)\ln(\alpha_{i,i-1}/\alpha_{i-1,i})$ with $G_1 \equiv 0$ by convention. Therefore $r_i r_{i+1} \cdots r_k = \exp(-\beta(G_{i-1} - G_k)$, and $X = r_1 r_2 \cdots r_s = \exp(-\beta \Delta G_{\mathrm{driv}})$. Eq. (22) can therefore be rewritten in terms of free energies as

$$
\frac{1}{J} = \frac{1}{1 - e^{-\beta \Delta G_{\mathrm{driv}}}}\left[\sum_{i=1}^{s}\sum_{j=1}^{s} \frac{e^{-\beta(G_{i-j} - G_i)}}{\alpha_{i,i+1}}\right] \qquad (23)
$$

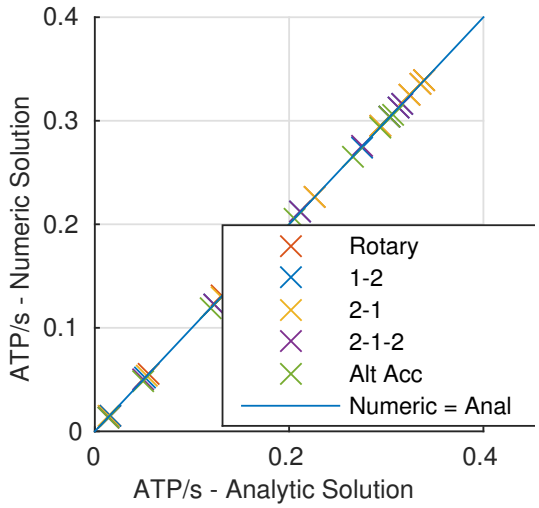

Figure S2: Comparison of the exact analytic NESS solution, Eq. (23), to the numeric solution obtained using Matlab.

For $i-j<1, G_{i-j}=G_{s-(i-j)}+\Delta G_{\text{driv}}$ which represents the free energy of the state corresponding to $s-(i-j)$ in the previous cycle. The analytic solution (Eq. (23)) is of course exactly the same as numerically solving the system of linear equations (Eq. (8)), within the limits of numerical accuracy. Figure S2 provides a numeric validation of the solution for all five ATP synthase cycles shown in Fig. S1.

4. Range of conditions

The range of values considered, for the physiological conditions driving ATP synthesis, were based on the values reported in the literature [8, 9, 10]. These ranges were extended beyond the reported ranges to represent potentially evolutionary and pathological states that may be more extreme than typical physiological conditions. The ranges used in this study are shown in Table S1. Note that pH_{out} represents the cytoplasmic pH value for *E. coli* ATP synthase and the matrix pH value for mitochondrial ATP synthase, consistent with the definition in [4]. During ATP synthesis ions are transport form the "in" side of the membrane to the "out" side, so $\Delta\text{pH}=\text{pH}_{\text{out}}-\text{pH}_{\text{in}}$ and $\Delta\psi=\psi_{\text{out}}-\psi_{\text{in}}$. Conditions within the range of values shown in Table S1, with the exception of ΔG_{driv} and ΔG^0 (Eq. 3), were randomly sampled for the parameter optimization protocol, described in Methods in the main text, and for the test results shown in the main text and in here. Any conditions that resulted in a driving potential outside the range of values shown in Table S1 were excluded from the analysis. The concentration values for ADP and Pi were sampled in log space and all other values were sampled in linear space.

5. Range of parameter values

Although the "Max-Min" protocol, described in the main text, does not require parameter values to be specified, the range of realistic values are limited by physical and structural constraints [11, 12]. The parameter values for F-ATPase reported in the literature vary considerably [13, 14, 15, 16, 17, 18, 19]. For the purpose of this analysis we use an optimization range spanning one order of magnitude around a representative set of values chosen from the literature, as shown in Table S2. Each step in the process shown in Fig. S1 has a binding k_{on} (or forward k_{dt} in the case of ADP phosphorylation) and an unbinding k_{off} (or reverse k_{td}) rate constant. $K_d=k_{\text{off}}/k_{\text{on}}$ and $K^{dt}=k_{dt}/k_{td}$ are the dissociation constants and the equilibrium constant for ADP to ATP phosphorylation, respectively. We also defined a cooperativity factor β, which represents the cooperativity between the proton binding sites, i.e. the effect of the (un)binding of one H^+ on the binding affinity of a subsequent H^+. Specifically, $K_d^{H^+_{\text{in2}}}=K_d^{H^+_{\text{in1}}}10^{\beta_{\text{in1}}}$, $K_d^{H^+_{\text{in3}}}=K_d^{H^+_{\text{in2}}}10^{\beta_{\text{in2}}}$, $K_d^{H^+_{\text{out2}}}=K_d^{H^+_{\text{out1}}}10^{\beta_{\text{out1}}}$, and $K_d^{H^+_{\text{out3}}}=K_d^{H^+_{\text{out2}}}10^{\beta_{\text{out2}}}$.

Table S1: Range of conditions. Ranges based on reported physiological conditions for *E. coli* and mitochondrial ATP synthase [8]. Also listed are the condition values used for Figs. 3 and 4 of the main text. Note that pH_{out}represents the cytoplasmic pH value for *E. coli* ATP synthase and the matrix pH value for mitochondrial ATP synthase, consistent with the definition in [4], $\Delta pH = pH_{out} - pH_{in}$, and $\Delta\psi = \psi_{out} - \psi_{in}$.

Condition	Literature [8]	Range used	Values for Figs. 3 & 4 of main text
pH_{out}	7.7 – 8.2	6.5–8.5	7.5
[ATP]/[ADP]	2.6 – 10.0	1 – 10	5.5
ΔpH	0.6 – 2.5	0 – 2	1
$\Delta\psi$(mV)	-80 – -220	0 – -250	-125
[ADP] (M)	8×10^{-3}	$8 \times 10^{-2} - 8 \times 10^{-4}$	8×10^{-2}
[Pi] (mM)	1 – 240	1 – 240	120
ΔG_{driv} (kcal/mol)	0 – 8	0 – 8	
ΔG^0 (kcal/mol)	7.6	7.6	7.6

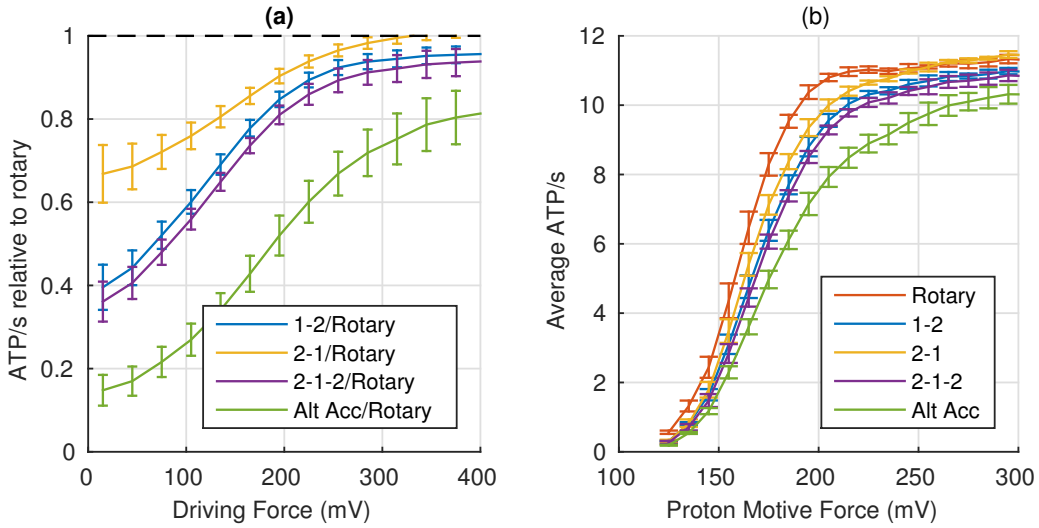

Figure S3: Results for baseline (default) model assumptions (3:1 H^+:ATP stoichiometry). (a) Geometric average ratio of ATP/s relative to rotary mechanism. (b) Average rate of ATP synthesis. See Table S3 for baseline model assumptions. Error bars show the standard error of the mean when sampling over a range of conditions. Connecting lines are shown to guide the eye.

6. Sensitivity analysis

Extensive systematic sensitivity analysis shows that our results are qualitatively insensitive to model assumptions (Table S3, Fig. S3 – S11). The model assumptions include event order (reaction sequence), optimization protocol for kinetic parameters, optimized parameter values, and the range of values for pH on the high pH side of the membrane, pH_{out}. The baseline (default) set of model assumptions are shown in the first row of data in Table S3, and the corresponding results in Fig. S3. All results are based on five sets of >10000 random conditions sampled from the range of values shown in Table S1 as described in the *Range of conditions* section above.

In addition to the baseline event order (Fig. S1), tests of six other event orders (model assumptions 2 – 7 in Table S3) show that the results are qualitatively insensitive to event order (Fig. S4 and S5). In the table, "Free" refers to the free ATP synthase after ATP release, "ADP" refers to ADP binding, "Pi" refers to Pi binding, "dt" refers to the phosphorylation of ADP to ATP, and "3×H^+" refers to the transport of three protons in the order shown in Fig. S1 for the different mechanisms. We also considered one event order where the H^+ binding/unbinding is interspersed with the other events (model asumption 7 in Table S3). In this case "H^+" refers to two of the proton binding or unbinding steps shown in Fig. S1 corresponding to each of the five mechanisms, e.g. for the rotary mechanism each H^+ refers to the transport (binding on the in-side and unbinding on the out-side) of a proton, whereas for the alternating access mechanism the first

Table S2: Parameter ranges for optimization. k_{on} are the binding rate constants, K_d the dissociation constants, k_{dt} and K^{dt} the ADP phosphorylation rate and equilibrium constants, and β represents the cooperativity factor between consecutive H^+binding and transport as described in the text. Also listed are the parameter values used for Figs. 3 and 4 of the main text. The thermodynamic cycle constraint, described above, is used to calculate the value for $K_{\text{off}}^{H_{\text{in}}^+}$.

Parameter	Literature	Value/Range used	Values for Figs. 3 & 4 of main text
k_{on}^{Pi} (M^{-1} s^{-1})	12 [14]	$1 - 10^2$	10^2
k_{on}^{ADP} (M^{-1} s^{-1})	4.2×10^6 [14]	$4 \times 10^5 - 4 \times 10^7$	4×10^7
k_{on}^{ATP} (M^{-1} s^{-1})	4.0×10^7 [14]	$4 \times 10^6 - 4 \times 10^8$	4×10^8
$k_{\text{on}}^{H_{\text{in}}^+}$ (M^{-1} s^{-1})	4×10^{10} [13]	$4 \times 10^9 - 4 \times 10^{11}$	4×10^{11}
$k_{\text{on}}^{H_{\text{out}}^+}$ (M^{-1} s^{-1})	4×10^{10} [13]	$4 \times 10^9 - 4 \times 10^{11}$	4×10^{11}
K_d^{Pi} (M)	17 [14]	$2 - 2 \times 10^2$	2
K_d^{ADP} (M)	8.6×10^{-5} [14]	$9 \times 10^{-4} - 9 \times 10^{-6}$	9×10^{-6}
K_d^{ATP} (M)	4.9×10^{-4} [14]	$5 \times 10^{-3} - 5 \times 10^{-5}$	5×10^{-3}
$K_d^{H_{\text{in}}^+}$ (M)	1.6×10^{-6} [18]	Thermodynamic Constraint	
$K_d^{H_{\text{out}}^+}$ (M)	1.6×10^{-8} [18]	$2 \times 10^{-7} - 2 \times 10^{-9}$	2×10^{-7}
k_{dt} (s^{-1})	120 [14]	$10 - 10^3$	10^3
K^{dt}	0.9 [14]	0.1 - 10	10
$10^{\beta_{\text{in1}}}$		$10^{-1} - 10^{+1}$	10^{+1}
$10^{\beta_{\text{out1}}}$		$10^{-1} - 10^{+1}$	10^{+1}
$10^{\beta_{\text{in2}}}$		$10^{-1} - 10^{+1}$	$10^{+0.2}$
$10^{\beta_{\text{out2}}}$		$10^{-1} - 10^{+1}$	10^{-1}

H^+ refers to the binding of the first two protons, the second H^+ refers to the binding of the third proton and unbinding of the first, and the third H^+ refers to the unbinding of the remaining two protons.

The evolution-inspired optimization protocol separately optimizes the parameters for each mechanism, *without fitting*, to maximize the rate of ATP synthesis under challenging conditions [20]. See Methods in the main text. The baseline optimization protocol selects the lower 10 percentile of parameter sets (models) characterizing the "challenging conditions" (Fig. S3). Tests of three additional characterizations of challenging conditions, the lower 0 percentile, 20 percentile and 50 percentile, show that the results are qualitatively insensitive to event order (Fig. S6 and S7).

In addition to the parameters determined by the optimization protocol, we tested five different randomly generated sets of parameter values. The range of realistic values are limited by physical and structural constraints [11, 12]. For the purpose of this analysis the parameters values were sampled from a uniform distribution in log space in the vicinity (± 1 order of magnitude) of the literature values (Table S2). The results are qualitatively insensitive to parameter values (Fig. S8 and S9), These random set of parameter values are listed in Table S4.

We also considered three pH_{out} ranges: 5.5–7.5, 6.5–8.5 and 7.5–9.5 showing that the results are qualitatively insensitive to pH_{out} range (Fig. S10 and S11). Since the FE of ATP synthesis ΔG^0 depends on pH [5], we use different values for the three different ranges approximately representing the average value for ΔG^0 within the range of pH values: 6.7 kcal/mol for 5.5–7.5, 7.6 kcal/mol for 6.5–8.5, and 8.3 for 7.5–9.5.

Each set of model assumptions was tested for the full range of operating conditions and the results were qualitatively similar. Table S3 and Fig. S3–S11 show that the results are qualitatively insensitive to model assumptions, with the rotary mechanism, on average, being faster than other possible mechanisms and exhibiting a sigmoidal relationship between rate and pmf as seen in experiments [4]. These results are summarized in Fig. 2(a) of the main text.

Table S3: Summary data from sensitivity analysis. Performance of possible alternative mechanisms relative to the rotary mechanism for different model assumptions. Average ratio is geometric average of ATP/s relative to rotary mechanism. Model assumption 1 represents the baseline (default) model corresponding to results shown in Fig. S3. The Event Orders and Parameter Ranges are described in the text.

Model assumptions					Average ATP/s ratio			
Id	Event order	Opt. protocol	Parameter ranges	pH_{out} ranges	$\frac{1-2}{\text{rotary}}$	$\frac{2-1}{\text{rotary}}$	$\frac{2-1-2}{\text{rotary}}$	$\frac{\text{alt acc}}{\text{rotary}}$
1	- Free - ADP - Pi - 3×H^+- dt - Free - (Fig. S1)	10%	From literature (Table S2)	6.5–8.5	0.82	0.94	0.80	0.60
2	- Free - Pi - ADP - 3×H^+- dt - Free -	—"—	—"—	—"—	0.94	0.91	0.91	0.75
3	- Free - ADP - 3×H^+- Pi - dt - Free -	—"—	—"—	—"—	0.94	0.91	0.85	0.66
4	- Free - Pi - 3×H^+- ADP - dt - Free -	—"—	—"—	—"—	0.89	0.97	0.90	0.71
5	- Free - 3×H^+- ADP - Pi - dt - Free -	—"—	—"—	—"—	0.95	0.82	0.83	0.63
6	- Free - 3×H^+- Pi - ADP - dt - Free -	—"—	—"—	—"—	0.73	0.85	0.72	0.49
7	- Free - H^+- ADP - H^+- Pi -H^+- dt - Free	—"—	—"—	—"—	0.62	0.75	0.59	0.73
8	- Free - ADP - Pi - 3×H^+- dt - Free - (Fig. S1)	0%	From literature (Table S2)	6.5–8.5	0.72	0.82	0.66	0.37
9	—"—	20%	—"—	—"—	0.75	0.88	0.74	0.51
10	—"—	50%	—"—	—"—	0.72	0.87	0.73	0.54
11	- Free - ADP - Pi - 3×H^+- dt - Free - (Fig. S1)	10%	Random set 1	6.5–8.5	0.94	0.90	0.86	0.51
12	—"—	—"—	Random set 2	—"—	0.81	0.97	0.78	0.71
13	—"—	—"—	Random set 3	—"—	0.94	0.94	0.87	0.64
14	—"—	—"—	Random set 4	—"—	0.98	0.97	0.95	0.86
15	—"—	—"—	Random set 5	—"—	0.91	0.92	0.83	0.76
16	- Free - ADP - Pi - 3×H^+- dt - Free -	10%	From literature (Table S2)	5.5–7.5	0.87	0.95	0.84	0.53
17	—"—	—"—	—"—	7.5–8.5	0.71	0.83	0.67	0.36

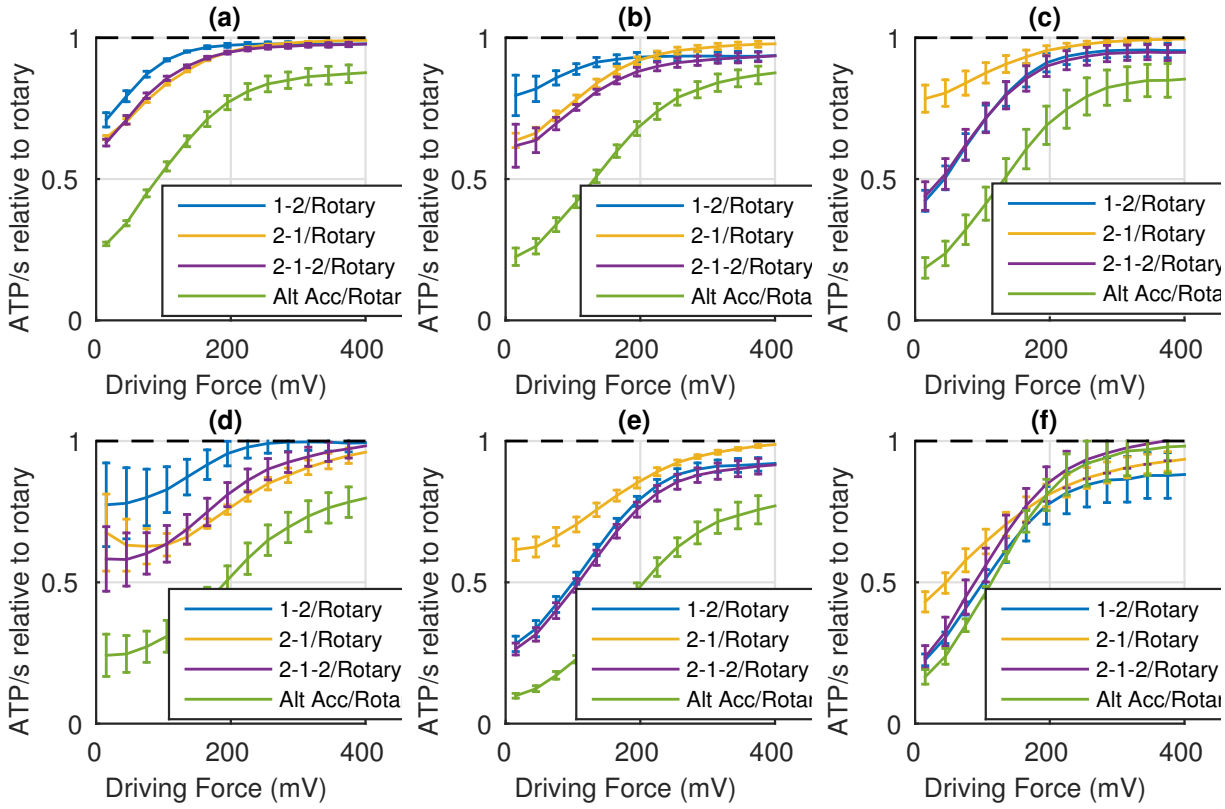

Figure S4: Sensitivity to event order (3:1 H^+:ATP stoichiometry). (a) – (f) show the geometric average ratio relative to the rotary mechanism, for event orders corresponding to model assumption 2 – 7 in Table S3. Results are qualitatively similar to the results for the baseline event order shown in Fig. S3. Error bars show the standard error of the mean when sampling over a range of conditions. Connecting lines are shown to guide the eye.

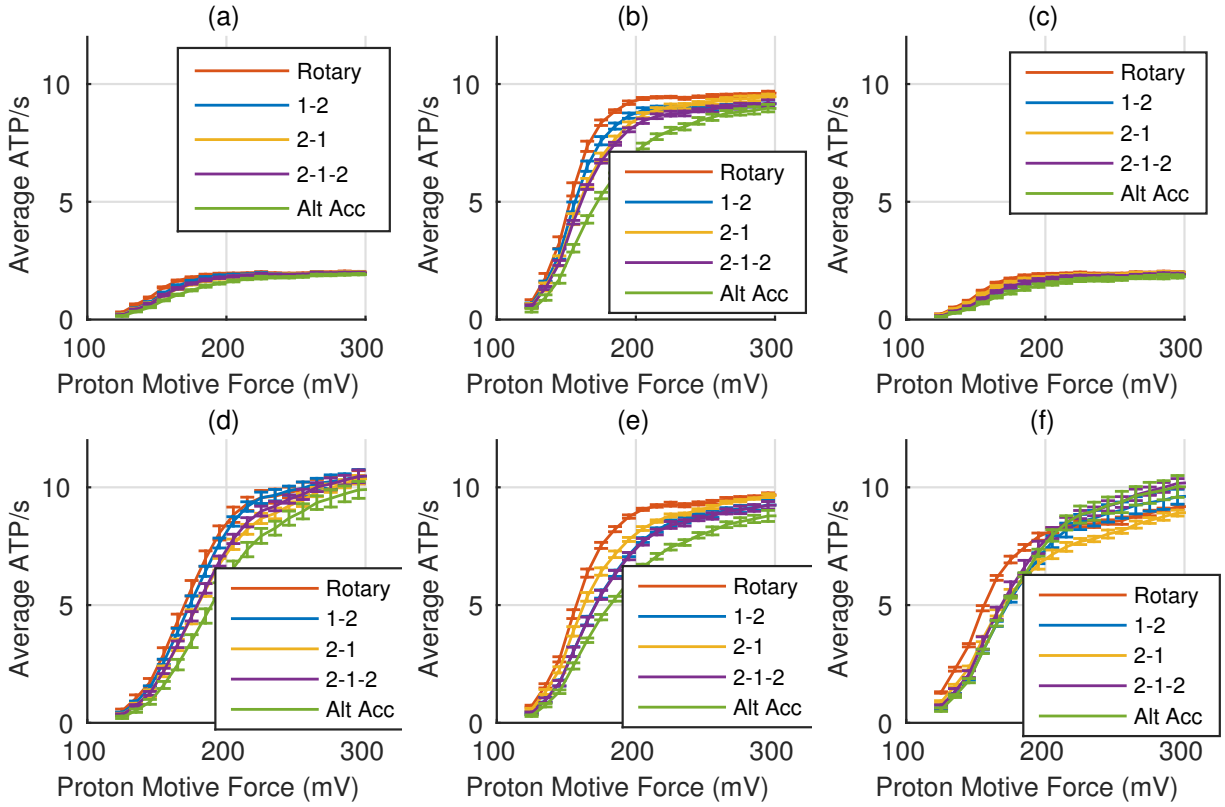

Figure S5: Sensitivity of rate of ATP synthesis to event order (3:1 H^+:ATP stoichiometry). (a) – (f) show the average ATP/s for event orders corresponding to model assumption 2 – 7 in Table S3. Results are qualitatively similar to the results for the baseline event order shown in Fig. S3. Error bars show the standard error of the mean when sampling over a range of conditions. Connecting lines are shown to guide the eye.

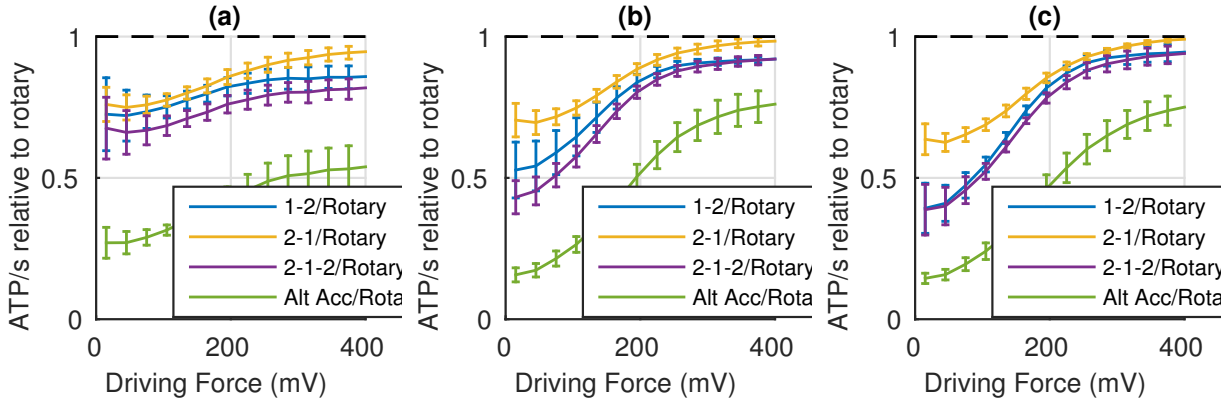

Figure S6: Sensitivity to optimization protocol (3:1 H^+:ATP stoichiometry). Geometric average ratio relative to the rotary mechanism for the lower (a) 0 percentile, (b) 20 percentile, and (c) 50 percentile of parameter sets characterizing the challenging condition, corresponding to model assumptions 8 – 10 in Table S3. Results are qualitatively similar to the results for the baseline optimization protocol shown in Fig. S3. Error bars show the standard error of the mean when sampling over a range of conditions. Connecting lines are shown to guide the eye.

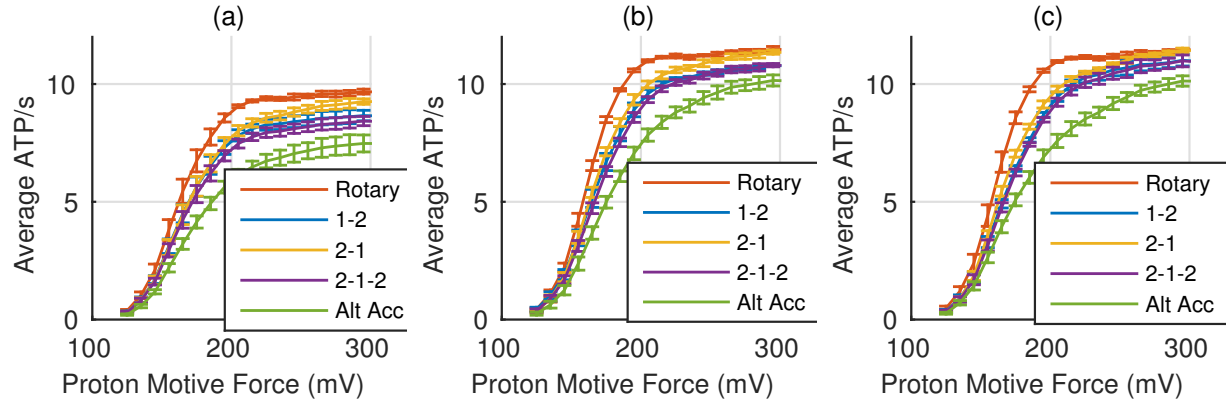

Figure S7: Sensitivity of rate of ATP synthesis to optimization protocol (3:1 H^+:ATP stoichiometry). Average ATP/s for the lower (a) 0 percentile, (b) 20 percentile, and (c) 50 percentile of parameter sets characterizing the challenging condition, corresponding to model assumptions 8 – 10 in Table S3. Results are qualitatively similar to the results for the baseline optimization protocol shown in Fig. S3. Error bars show the standard error of the mean when sampling over a range of conditions. Connecting lines are shown to guide the eye.

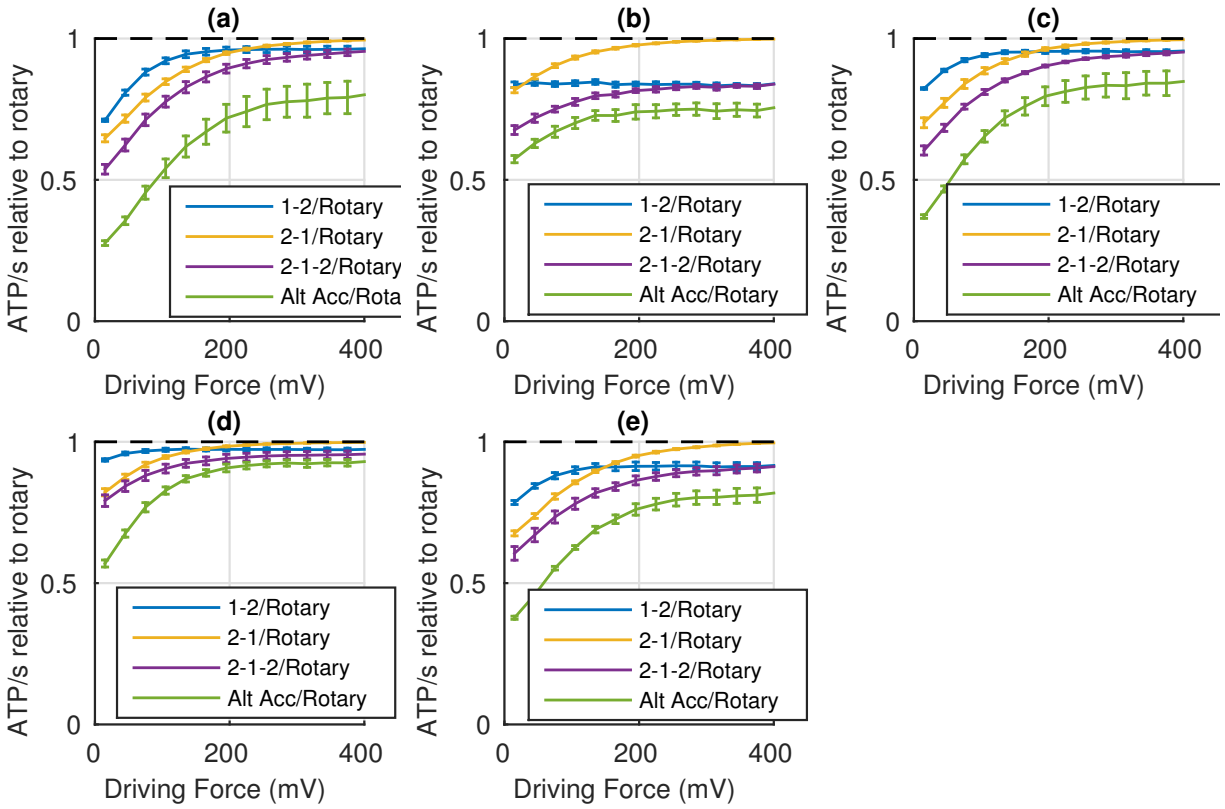

Figure S8: Sensitivity to parameter values (3:1 H^+:ATP stoichiometry). (a) – (e) show the geometric average ratio relative to the rotary mechanism, for random sets of parameter values corresponding to random sets 1 – 5 in Table S4. Results are qualitatively similar to the results for the baseline parameter values shown in Fig. S3. Error bars show the standard error of the mean when sampling over a range of conditions. Connecting lines are shown to guide the eye.

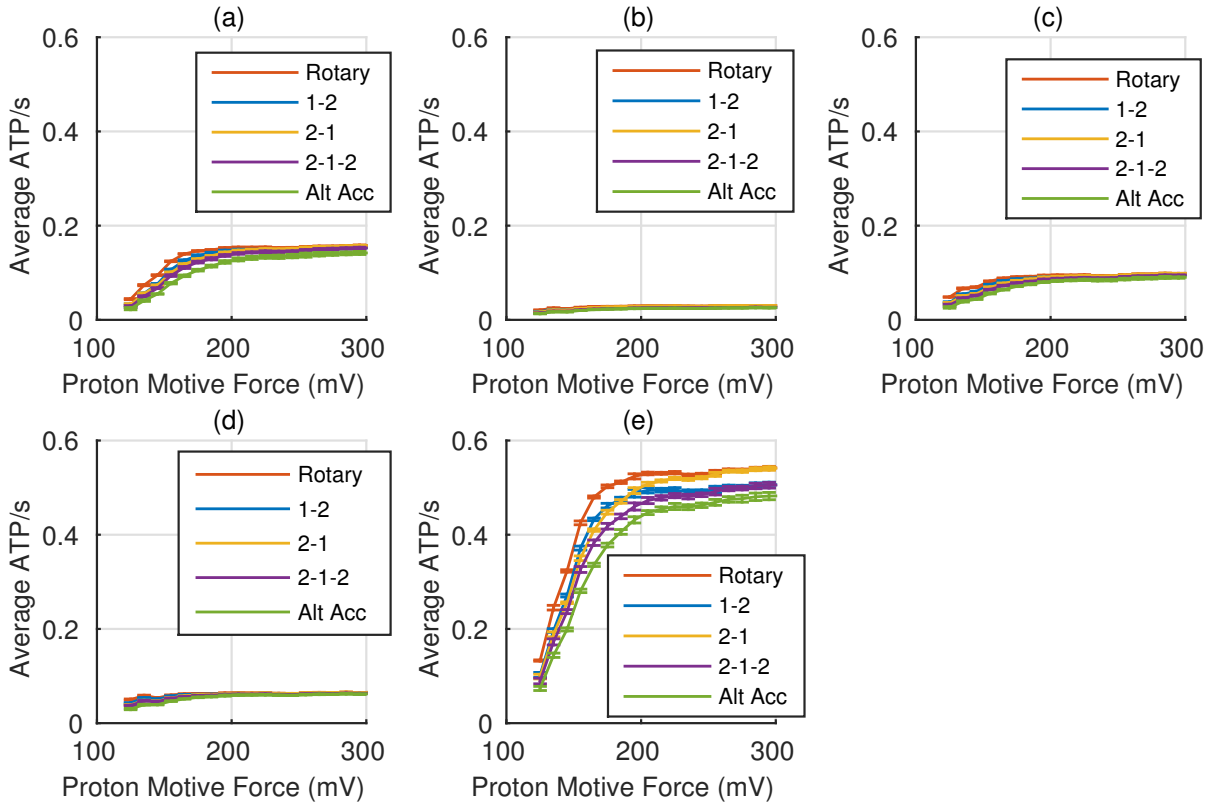

Figure S9: Sensitivity of rate of ATP synthesis to parameter values (3:1 H^+:ATP stoichiometry). (a) – (e) show the average rate for random sets of parameter values corresponding to random sets 1 – 5 in Table S4. Results are qualitatively similar to the results for the baseline parameter values shown in Fig. S3. Error bars show the standard error of the mean when sampling over a range of conditions. Connecting lines are shown to guide the eye.

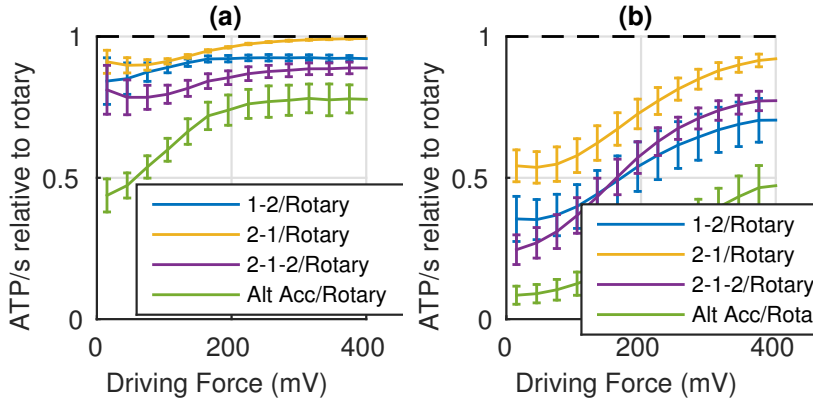

Figure S10: Sensitivity to pH_{out} (3:1 H^+:ATP stoichiometry). Geometric average ratio relative to the rotary mechanism for the pH_{out} range of (a) 5.5 – 7.5 and (b) 7.5 – 9.5, corresponding to model assumptions 16 and 17 in Table S3, respectively. Results are qualitatively similar to the results for the baseline pH range shown in Fig. S3. Error bars show the standard error of the mean when sampling over a range of conditions. Connecting lines are shown to guide the eye.

Table S4: Random set of parameter values used for sensitivity analysis.

Parameter	Random set 1	Random set 2	Random set 3	Random set4	Random set 5
k_{on}^{Pi} (M^{-1} s^{-1})	$10^{0.61}$	$10^{0.87}$	$10^{1.02}$	$10^{1.43}$	$10^{1.84}$
k_{on}^{ADP} (M^{-1} s^{-1})	$4 \times 10^{5.29}$	$4 \times 10^{5.84}$	$4 \times 10^{6.79}$	$4 \times 10^{6.40}$	$4 \times 10^{5.98}$
k_{on}^{ATP} (M^{-1} s^{-1})	$4 \times 10^{6.19}$	$4 \times 10^{6.66}$	$4 \times 10^{7.79}$	$4 \times 10^{6.43}$	$4 \times 10^{7.22}$
$k_{\text{on}}^{H_{\text{in}}^+}$ (M^{-1} s^{-1})	$4 \times 10^{9.37}$	$4 \times 10^{9.41}$	$4 \times 10^{9.25}$	$4 \times 10^{10.95}$	$4 \times 10^{10.53}$
$k_{\text{on}}^{H_{\text{out}}^+}$ (M^{-1} s^{-1})	$4 \times 10^{9.37}$	$4 \times 10^{9.41}$	$4 \times 10^{9.25}$	$4 \times 10^{10.95}$	$4 \times 10^{10.53}$
K_d^{Pi} (M)	$2 \times 10^{0.83}$	$2 \times 10^{0.87}$	$2 \times 10^{1.10}$	$2 \times 10^{1.93}$	$2 \times 10^{0.44}$
K_d^{ADP} (M)	$9 \times 10^{-5.44}$	$9 \times 10^{-4.05}$	$9 \times 10^{-5.42}$	$9 \times 10^{-5.10}$	$9 \times 10^{-5.74}$
K_d^{ATP} (M)	$5 \times 10^{-3.00}$	$5 \times 10^{-4.10}$	$5 \times 10^{-3.58}$	$5 \times 10^{-4.95}$	$5 \times 10^{-3.41}$
$K_d^{H_{\text{out}}^+}$ (M)	$2 \times 10^{-7.69}$	$2 \times 10^{-8.24}$	$2 \times 10^{-7.42}$	$2 \times 10^{-7.01}$	$2 \times 10^{-8.04}$
k_{dt} (s^{-1})	119.57	34.18	76.14	74.06	23.74
K^{dt}	0.62	0.13	0.40	0.32	0.39

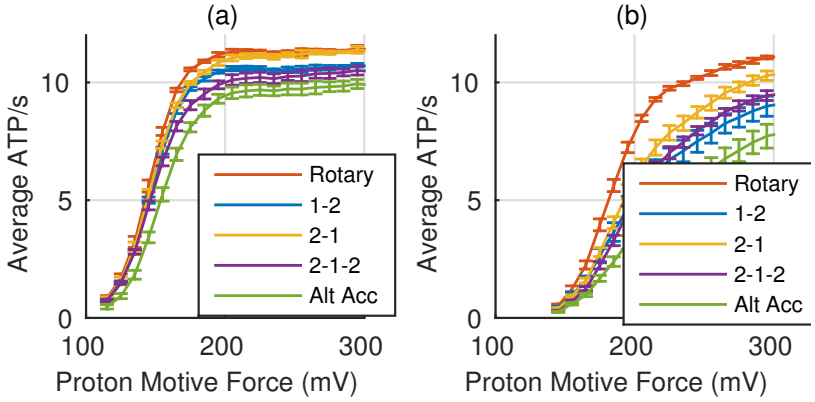

Figure S11: Sensitivity of rate of ATP synthesis to pH_{out} (3:1 H^+:ATP stoichiometry). Average ATP/s for the pH_{out} range of (a) 5.5 – 7.5 and (b) 7.5 – 9.5, corresponding to model assumptions 16 and 17 in Table S3, respectively. Results are qualitatively similar to the results for the baseline pH range shown in Fig. S3. Error bars show the standard error of the mean when sampling over a range of conditions. Connecting lines are shown to guide the eye.

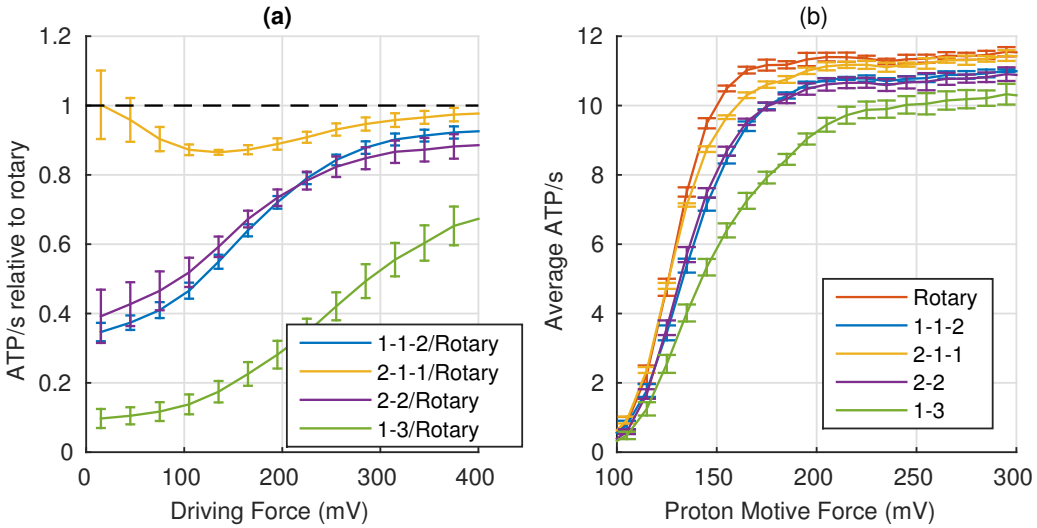

Figure S12: Test of 4:1 H^+:ATP stoichiometry. (a) Geometric average ratio of ATP/s relative to rotary mechanism. (b) Average rate of ATP synthesis. Results are qualitatively similar to the results for the 3:1 stoichiometry shown in Fig. S3. Error bars show the standard error of the mean when sampling over a range of conditions. Connecting lines are shown to guide the eye.

7. Test of 4:1 H^+:ATP stoichiometry

For the results shown above we chose a 3:1 H^+:ATP stoichiometry, approximately representative of *E. coli* and animal mitochondria ATP synthase [8]. Other species use higher stoichiometries, e.g. 4:1 for *T. Thermophilius* [21], 4.7:1 for chloroplast [22] and 5:1 for *S. Platnesis* [23] ATP synthase. Fig. S12 shows that the results for a 4:1 stoichiometry are qualitatively similar to the results for the 3:1 stoichiometry. We selected five of the 14 possible proton binding/unbinding orders for this analysis: the rotary mechanism with one-at-a-time H^+transport ($+H^+$ $-H^+$ $+H^+$ $-H^+$ $+H^+$ $-H^+$ $+H^+$ $-H^+$), the "1-1-2" mechanism ($+H^+$ $-H^+$ $+H^+$ $-H^+$ $+H^+$ $+H^+$ $-H^+$ $-H^+$), the "2-1-1" mechanism ($+H^+$ $+H^+$ $-H^+$ $-H^+$ $+H^+$ $-H^+$ $+H^+$ $-H^+$), the "2-2" mechanism ($+H^+$ $+H^+$ $-H^+$ $-H^+$ $+H^+$ $+H^+$ $-H^+$ $-H^+$), and the "1-3" mechanism ($+H^+$ $+H^+$ $+H^+$ $-H^+$ $+H^+$ $-H^+$ $-H^+$ $-H^+$), where $+H^+$ refers to proton binding on the in-side and $-H^+$ to proton unbinding on the out-side of the membrane. The same range of conditions and parameters shown in Tables S1 and S2 were used here, although some of the conditions may not be as representative for the 4:1 H^+:ATP stoichiometry.

References

[1] Wolfgang Junge and Nathan Nelson. ATP Synthase. *Annu. Rev. Biochem.*, 84(1):631–657, 2015.

[2] Kazuhiro Abe, Kazutoshi Tani, Tomohiro Nishizawa, and Yoshinori Fujiyoshi. Inter-subunit interaction of gastric H+,K+-ATPase prevents reverse reaction of the transport cycle. *EMBO J.*, 28(11):1637–1643, June 2009.

[3] Terrell L. Hill. *Free Energy Transduction and Biochemical Cycle Kinetics*. Dover Publications, December 2004.

[4] Naoki Soga, Kazuhiko Kinosita, Masasuke Yoshida, and Toshiharu Suzuki. Kinetic Equivalence of Transmembrane pH and Electrical Potential Differences in ATP Synthesis. *J. Biol. Chem.*, 287(12):9633–9639, March 2012.

[5] Robert A. Alberty. Effect of pH and Metal Ion Concentration on the Equilibrium Hydrolysis of Adenosine Triphosphate to Adenosine Diphosphate. *J. Biol. Chem.*, 243(7):1337–1343, April 1968.

[6] Jeff Boork and Håkan Wennerström. The influence of membrane potentials on reaction rates. Control in free-energy-transducing systems. *Biochim. Biophys. Acta, Bioenerg.*, 767(2):314–320, November 1984.

[7] Yann R. Chemla, Jeffrey R. Moffitt, and Carlos Bustamante. Exact Solutions for Kinetic Models of Macromolecular Dynamics. *J. Phys. Chem. B*, 112(19):6025–6044, May 2008.

[8] Todd P. Silverstein. An exploration of how the thermodynamic efficiency of bioenergetic membrane systems varies with c-subunit stoichiometry of F1F0 ATP synthases. *J. Bioenerg. Biomemb.*, 46(3):229–241, 2014.

[9] Dmitry Akhmedov, Matthias Braun, Chikage Mataki, Kyu-Sang Park, Tullio Pozzan, Kristina Schoonjans, Patrik Rorsman, Claes B. Wollheim, and Andreas Wiederkehr. Mitochondrial matrix pH controls oxidative phosphorylation and metabolism-secretion coupling in INS-1E clonal Îš cells. *FASEB J.*, 24(11):4613–4626, November 2010.

[10] S. Soboll, R. Scholz, and H. W. Heldt. Subcellular metabolite concentrations. Dependence of mitochondrial and cytosolic ATP systems on the metabolic state of perfused rat liver. *Eur. J. Biochem. FEBS*, 87(2):377–390, June 1978.

[11] Magnus Johansson, Martin Lovmar, and Måns Ehrenberg. Rate and accuracy of bacterial protein synthesis revisited. *Curr. Opin. Microbiol.*, 11(2):141–147, April 2008.

[12] Athel Cornish-Bowden. *The Pursuit of Perfection: Aspects of Biochemical Evolution*. Oxford University Press, 1st edition, November 2004.

[13] O. A. Gopta, D. A. Cherepanov, W. Junge, and A. Y. Mulkidjanian. Proton transfer from the bulk to the bound ubiquinone Q(B) of the reaction center in chromatophores of Rhodobacter sphaeroides: retarded conveyance by neutral water. *Proc. Natl. Acad. Sci. U.S.A.*, 96(23):13159–13164, November 1999.

[14] Joanne A. Baylis Scanlon, Marwan K. Al-Shawi, Nga P. Le, and Robert K. Nakamoto. Determination of the Partial Reactions of Rotational Catalysis in F1-ATPase. *Biochem.*, 46(30):8785–8797, July 2007.

[15] Kengo Adachi, Kazuhiro Oiwa, Takayuki Nishizaka, Shou Furuike, Hiroyuki Noji, Hiroyasu Itoh, Masasuke Yoshida, and Kazuhiko Kinosita. Coupling of Rotation and Catalysis in F1-ATPase Revealed by Single-Molecule Imaging and Manipulation. *Cell*, 130(2):309–321, July 2007.

[16] Kengo Adachi, Kazuhiro Oiwa, Masasuke Yoshida, Takayuki Nishizaka, and Kazuhiko Kinosita. Controlled rotation of the F1-ATPase reveals differential and continuous binding changes for ATP synthesis. *Nat. Commun.*, 3:1022+, August 2012.

[17] C. Grubmeyer, R. L. Cross, and H. S. Penefsky. Mechanism of ATP hydrolysis by beef heart mitochondrial ATPase. Rate constants for elementary steps in catalysis at a single site. *J. Biol. Chem.*, 257(20):12092–12100, October 1982.

[18] Peter Gräber. The H+-ATPase from chloroplasts: Energetics of the catalytic cycle. *Biochim. Biophys. Acta, Bioenerg.*, 1187(2):171–176, August 1994.

[19] O. Panke and B. Rumberg. Kinetic modelling of the proton translocating CF0CF1-ATP synthase from spinach. *FEBS Lett.*, 383:196+, 1996.

[20] Yonatan Savir and Tsvi Tlusty. The Ribosome as an Optimal Decoder: A Lesson in Molecular Recognition. *Cell*, 153(2):471–479, April 2013.

[21] Masahiro Nakano, Hiromi Imamura, Masashi Toei, Masatada Tamakoshi, Masasuke Yoshida, and Ken Yokoyama. ATP Hydrolysis and Synthesis of a Rotary Motor V-ATPase from Thermus thermophilus. *J. Biol. Chem.*, 283(30):20789–20796, July 2008.

[22] Paola Turina, Jan Petersen, and Peter Gräber. Thermodynamics of proton transport coupled ATP synthesis. *Biochim. Biophys. Acta, Bioenerg.*, 1857(6):653–664, March 2016.

[23] Denys Pogoryelov, Ozkan Yildiz, Jose D. Faraldo-Gomez, and Thomas Meier. High-resolution structure of the rotor ring of a proton-dependent ATP synthase. *Nat. Struct. Mol. Biol.*, 16(10):1068–1073, October 2009.